

## **Non-radiative and radiative decays in nanogap emitting devices**

Rémi Faggiani, Jianji Yang, and Philippe Lalanne\*

Laboratoire Photonique Numérique et Nanosciences, Institut d'Optique d'Aquitaine, Université Bordeaux, CNRS, 33405 Talence, France

\* E-mail: [philippe.lalanne@institutoptique.fr](mailto:philippe.lalanne@institutoptique.fr)

### **Abstract**

By placing a quantum emitter in the mouths of nanogaps consisting of two metal nanoparticles nearly into contact, significant increases in emission rate are obtained. This mechanism is central in the design of modern plasmonic nanoantennas. However, due to the lack of general knowledge on the balance between the different decay rates in nanogaps (emission, quenching, and metal absorption), nanoantenna design is performed in a rather haphazard fashion and relies on repeated numerical calculations; general intuitive design recipes do not presently exist. With accurate and simple closed-form expressions for the quenching rate and the decay rate into gap plasmons, we provide a comprehensive analysis of nanogap light emitting devices in the limit of small gap thickness. We disclose that the total spontaneous emission rate of quantum emitters in nanometer-thin gaps can largely overcome quenching, for specifically selected metallic and insulator materials, regardless of the gap size. Furthermore, to help further designs, we propose a classification of nanogap emitting devices based on two important figures of merit, the emission rate acceleration and the extraction efficiency, and further position a whole family of state-of-the-art devices based on nanogaps formed by nanocubes laying on metallic substrates in the classification.

## 1. Introduction

Dielectric nanogaps in metals have unprecedented ability to concentrate light into deep-subwavelength volumes, which has propelled their use in a vast array of nanotechnologies and research topics (1, 2). For instance biological species can be manipulated at very low input powers by the field-gradients at nanogaps (3), photodetector with sizes well below the diffraction limit may be implemented with very fast response time (4), magnetic resonance supported by nanogap resonators can be utilized to realize negative-index metamaterials (5, 6), and feedgaps can be used to enhance the efficiency of high-harmonic nonlinear optical processes (7). The strongly confined field also profoundly alters light emission of quantum emitters placed in the nanogap by increasing optical excitation rates, modifying radiative and nonradiative decay rates, and altering emission directionality, leading to a new generation of ultra-compact nanoantenna architectures, such as bowties, spiral antenna, phased-array antenna (8), and to new applications for light-emitting devices (9), broadband single-photon sources (10-12), single-plasmon sources (13, 14), spasers or low-threshold nanolasers (15-17).

It is generally accepted that sub-wavelength architectures improve the exchange of optical energy with matter at the nanoscale by increasing the spontaneous emission (SE) rate by orders of magnitude. As shown by numerical calculations and experimental measurements, it is also accepted that this enhancement can be achieved with relatively good efficiencies, ~10-60% depending on the architecture. However the precise physical mechanisms that drive the emission of quantum emitters placed very close to metal surfaces in tiny gaps are not well understood. In particular, it is unclear from the literature why a good efficiency is achieved despite the proximity to the metal, why quenching is not the dominant decay channel, what is the ultimate efficiency, and whether this limit is impacted by the gap thickness or other parameters.

To further explore how optical antennas may lead to unprecedented regimes of light-matter interactions, it is important to first understand the different physical mechanisms at play when quantum emitters in nanogaps emit light in the immediate vicinity of metal surfaces and then draw a relationship between this basic situation and more complex problems of light emission and coupling with subwavelength architectures.

This is exactly the approach that is adopted in this work. Firstly in Section 2, we provide a thorough and quantitative analysis of the physics at play in 2D planar nanogap. So far, this has been discussed only with scattered numerical calculations performed for specific gap thicknesses and metal dielectric constants (11, 18, 19). In contrast, we derive a closed-form formula for the branching ratio between quenching and plasmon decays, and then clarify the key material and geometrical parameters that drive the ratio. Counterintuitively,

we evidence that the key parameters are the material permittivities, and not the gap thickness (at least for small thicknesses) and that the gap plasmon decay surpasses the quenching decay for nanogaps feed with high-refractive-index materials.

In Section 3, by considering nanogap antenna architectures as gap-plasmon Fabry-Perot resonators, we utilize the understanding gained in Section 2 to propose a classification of nanogap antenna architectures and infer general recipes for designing efficient nanogap devices that boost fluorescence at visible and infrared frequencies, while preserving high extraction efficiency.

Finally in Section 4, we analyze state-of-the-art nanogap emitting devices formed by tiny nanocubes laying on metal surfaces (10, 12). By scaling down the gap thickness and the cube dimensions to keep resonance in the visible, we are able to explore distinct behaviors within the same architecture family and to quantitatively discuss the general performance of every category of the classification proposed in Section 3.

Section 5 summarizes the main results and provides a concluding discussion.

## 2. Radiative and non-radiative decays in dielectric nanogaps

To start the analysis, let us consider the emission of a vertically-polarized molecule (treated as an electric dipole) buried in the middle of a polymer layer of thickness  $2d$  of a metal-insulator-metal (MIM) planar stack. Two channels are available for the decay. Either the molecule excites the gap plasmon modes of the planar stack or quenches by directly heating the metal. We denote by  $\gamma_{GSP}$  and  $\gamma_{quench}$  the corresponding normalized decay rates (all decay rates are normalized by the vacuum decay rate hereafter). Figure 1 summarizes the main trends for the decay rates for an emission wavelength at 650 nm and a silver nanogap. First we find that the direct decay in the metal,  $\gamma_{quench}$ , scales as  $d^{-3}$  as  $d \rightarrow 0$ . This scaling is understood from the local and static nature of quenching. Intuitively the quenching rate in a nanogap is expected to be  $\sim 2$  times larger than the quenching rate  $\gamma_{quench}^{SI}$  of the same vertical dipole on a single interface at the same separation distance  $d$ , and

since  $\gamma_{quench}^{SI} = \frac{3}{8\varepsilon_d(k_0 d)^3} \text{Im} \left( \frac{\varepsilon_m - \varepsilon_d}{\varepsilon_m + \varepsilon_d} \right)$  as  $d \rightarrow 0$  (19), the cubic scaling is well

anticipated. In fact, as shown by,  $\gamma_{quench} \approx 2\gamma_{quench}^{SI}$  for  $d > 10$  nm only; as smaller  $d$ 's, we found empirically with numerical calculations performed at 650 nm that the quenching rate  $\gamma_{quench}$  is  $\sim 3$  times larger than  $\gamma_{quench}^{SI}$ .

Interestingly too, we find that the normalized decay rate  $\gamma_{GSP}$  into the gap plasmon modes of the planar stack also scales as the cube of the separation distance  $2d$  between the metal films. This scaling is less intuitively obvious since it results from an increase of the gap-plasmon local density of optical states which is boosted by an in-plane continuum of slow gap plasmons as  $d$  vanishes. But actually, it can be understood by considering that as  $d \rightarrow 0$ , gap plasmons completely lose their photonic character and become of the same nature as quenching, and thus the gap plasmon and quenching decay rate should scale in the same way. By using a complex continuation technique to calculate the Green-tensor (20) and by assuming that the transverse electric and magnetic field components of the gap plasmon bear a flat profile within the gap and penetrate into the metal cladding, we can derive an analytical expression for  $\gamma_{GSP}$  for very small gap thickness,  $\gamma_{GSP} \approx \frac{12\pi\epsilon_d}{(2k_0d)^3|\epsilon_m|^2}$  (see

Supporting Information for details), which evidences the inverse-cubic scaling.

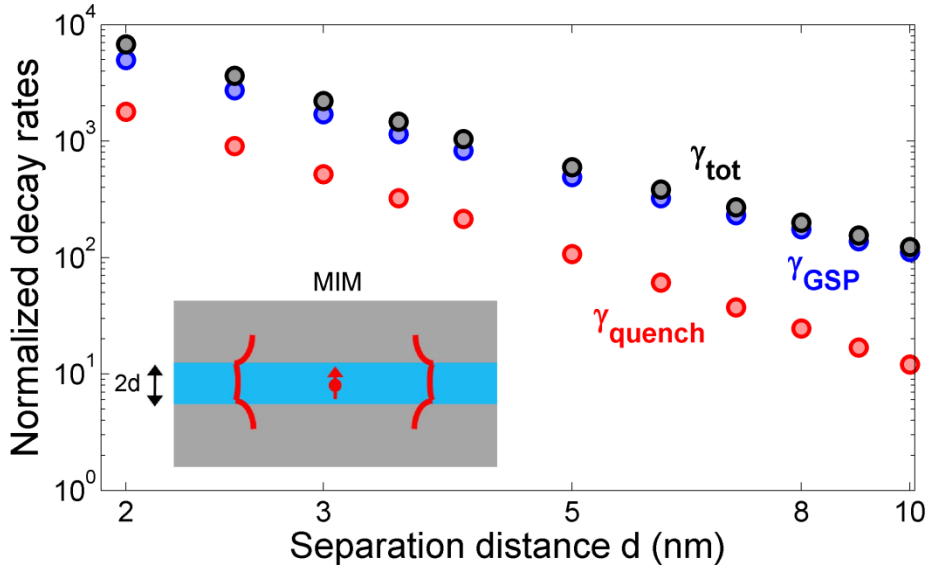


**Figure 1. Competition between several decay channels** for a vertical electric dipole emitting in the center of an Ag/polymer/Ag gap of width  $2d$ . The calculations are performed for an emission wavelength  $\lambda_0 = 650$  nm. The refractive index of polymer is  $n = 1.4$  and the silver permittivity is  $\epsilon_{Ag} = -17 + 1.15i$  (21). The decay

rates into all channels  $\gamma_{tot}$ , plasmonic modes  $\gamma_{GSP}$  and quenching  $\gamma_{quench}$  are shown with black, blue, and red circles, respectively. All the decay rates are normalized by the decay rate in the vacuum.

Thus we obtain an analytical expression for an important figure of merit of planar nanogaps with vanishing gap thicknesses, namely the branching ratio  $F$  between gap-plasmon decay rates and quenching rates

$$F \approx \frac{\gamma_{GSP}}{3\gamma_{quench}^{SI}} = \frac{2\varepsilon_d}{\text{Im}(\varepsilon_m(\omega))} \left| \frac{\varepsilon_m(\omega) + \varepsilon_d}{\varepsilon_m(\omega)} \right|^2, \quad (1)$$

with  $\varepsilon_d$  and  $\varepsilon_m$  denoting the dielectric and metal permittivities. The formula carries important hints:

- First, the ratio is independent of  $d$  for  $k_0d \rightarrow 0$ , the first correction term being of order  $O(k_0d)^2$ , and takes a universal expression that only depends on the dielectric constants.
- Second, for good metals,  $\varepsilon_d \ll |\varepsilon_m(\omega)|$ , one should bury the quantum emitter in a high-index material to enhance the branching ratio in the near- and far-infrared spectral regions.
- Third, the ratio solely depends on the losses encountered in polarizing the material, i.e. on  $\text{Im}(\varepsilon_m(\omega))$ , and not on the usual quality factor  $\frac{-\text{Re}(\varepsilon_m)}{\text{Im}(\varepsilon_m)}$  of plasmonic materials, which gives an incontestable advantage to silver at visible frequencies, in comparison with gold or aluminum for instance.

**Figure 2** shows typical branching ratios that can be obtained in the visible and near-infrared spectral regions with different metals and gap materials. The usefulness of the simple formula in Eq. (1) is reinforced by its ability to provide quantitative predictions, as evidenced with the comparison with fully-vectorial computational data (shown with marks) obtained for planar nanogaps with small gap sizes ( $d=2$  nm). We emphasize that Eq. (1) is obtained in the asymptotic limit  $k_0d \rightarrow 0$ ; as the gap thickness increases beyond the

quasi-static approximation, the ratio  $F$  increases because quenching rapidly vanishes, and in this sense Eq. (1) actually sets a lower bound for the branching ratios. On overall, Eq. (1) represents a good compromise between simplicity or intuition and accuracy.

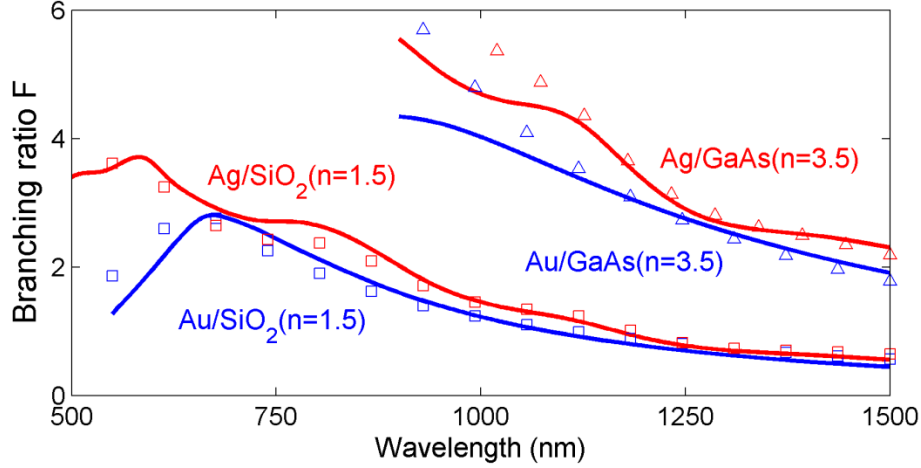


**Figure 2. Branching ratios for nanogaps formed with various materials at visible and near-infrared frequencies.** Fully-vectorial calculations (for  $d = 2$  nm) and analytical predictions from Eq. (1) are shown with markers and solid curves. Calculations made with Ag and Au are represented by red and blue colors, for dielectric (squares) and semiconductor (triangles) gap materials. Metal permittivities are taken from tabulated values (21).

In the fully-vectorial results shown in Figs. 1 and 2, quenching rates are found as the difference between the total decay rates and the decay rates into all the other channels (either plasmonic modes, or free-space radiative modes), which are rigorously calculated using an open-source software (22). Details on the calculation technique are provided in the SI along with a verification that the indirect derivation of the quenched energy actually corresponds to the absorption in the near-field zone ( $< 0.02\lambda_0^2$ ) of the emitter.

### 3. Classification of nanogap emission devices

Decay into plasmon modes is often considered to be detrimental, just like quenching. However it is of different nature, since plasmons are coherent oscillations that may be transformed into free-space photons by scattering. This transformation is at the art of nanogap-device design. Intuitively, gap device can be thought as Fabry-Perot nanoresonators with gap plasmon modes that bounce back and forth between two facets (23-25). We may

distinguish three different nanogap-device categories, according to the reflectivity  $R$  of the gap facets. The categories are illustrated in the classification of Fig. 3.

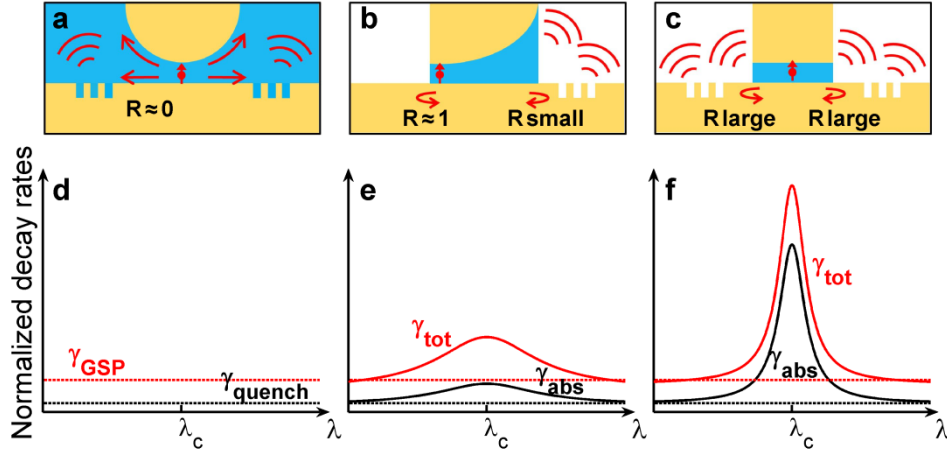


**Figure 3. Classification of planar nanogap emitting devices with different degrees of decay rate enhancements. (a)** Tapered devices with efficient extraction. Dipole emission is initially captured by gap plasmons and then adiabatically (low reflection  $R \sim 0$ ) extracted outside the device. **(b)** Nanoresonators with controlled reflections. **(c)** Nanoresonators with strong facet reflectivities. Grooves help conversion of launched SPPs into the free-space photons. **(d)-(f)** Corresponding decay rates. **(d)** Due to the tapering, the total decay rate  $\gamma_{tot}$  and the nonradiative decay rate  $\gamma_{abs}$  are expected to be comparable to the gap-plasmon and quenching decay rates obtained in a planar nanogap with a thickness equal to the mouth thickness,  $\gamma_{tot} \approx \gamma_{GSP} + \gamma_{quench}$  and  $\gamma_{abs} \approx \gamma_{quench}$ . **(e)** The weak reflection in **(b)** results in broadband rate enhancements with a large efficiency. **(f)** The strong reflection in **(c)** results in a narrowband FP resonance;  $\gamma_{tot}$  can be considerably boosted, but the non-radiative decay  $\gamma_{abs}$  due to cavity absorption lowers the extraction efficiency.

Almost nil reflectivity is implemented in tapered devices formed for instance by curved and flat metal surfaces (Fig. 3a) by adiabatically extracting the slow gap-plasmons generated at the mouth (26-28). Thus, the total decay rate  $\gamma_{tot}$  and the nonradiative decay rate  $\gamma_{abs}$  are expected to be

comparable to the gap-plasmon and quenching decay rates obtained in a planar nanogap with a thickness equal to the mouth thickness,  $\gamma_{tot} \approx \gamma_{GSP} + \gamma_{quench}$  and  $\gamma_{abs} \approx \gamma_{quench}$ ; large Purcell factors can be obtained for tiny gaps as shown in Fig. 1. The extraction efficiency (defined here as the ratio between the sum of the radiative and SPP decay rates and the total decay rate) is limited by quenching and therefore is bounded by  $F/(F+1)$ , a value that can be as large as 0.75 at an emission wavelength of 600 nm for Ag/polymer gaps (see Fig. 2).

By contrast, for strong reflectivity favored by large impedance mismatch at the facet of tiny gaps (10, 16), see the nanoresonators in Fig. 3c, the total decay rate is considerably boosted and quenching becomes completely negligible. However, the efficiency is limited by the non-radiative damping of gap plasmons in the tiny gap and is expected to be much smaller than the value reached for adiabatically-tapered antennas.

Figure 3b illustrates a promising class of nanogap antenna, with intermediate values of the facet reflectivity. Purcell factors larger than  $\gamma_{GSP}$  are implemented, but the efficiency that is limited by quenching and absorption in the cavity may approach or even exceed the upper bound value of the  $R \approx 0$  case.

#### 4. Performance of state-of-the-art nanocube devices

After this qualitative discussion, it is interesting to position current nanogap emitting-device technologies against the classification of Fig. 3, and in particular to position recent state-of-the-art realizations based on nanogaps formed by nanocubes laying on metallic substrates (10, 11). For this purpose, we first analyze the nanocube emitting device reported in (10), using exactly the same parameters as in the experiment; then by scaling down all the cube dimensions, we analyze a whole family of gap emitting devices with very distinct facet reflectivities, which all resonate at the same visible wavelength.

The nanogap emitting device reported in (10) is depicted in the left inset of Fig. 4 and the physical parameters are given in the caption. The emitting dipole is assumed to be vertically polarized and placed in the middle of an 8-nm-thick polymer gap at a cube corner (right inset), where maximum coupling with the resonance mode is achieved. Using COMSOL multiphysics, we first calculate the normalized total decay rate  $\gamma_{tot}$  by integrating the total

power radiated around the source. Consistently with (10),  $\gamma_{tot}$  (black circles) at resonance ( $\lambda_0 = 650$  nm) is as large as  $10^4$ , a value which represents a tenfold enhancement, compared to the normalized gap-plasmon decay  $\gamma_{GSP}$  (cyan circles) obtained for a planar nanogap with the same materials and gap thickness.

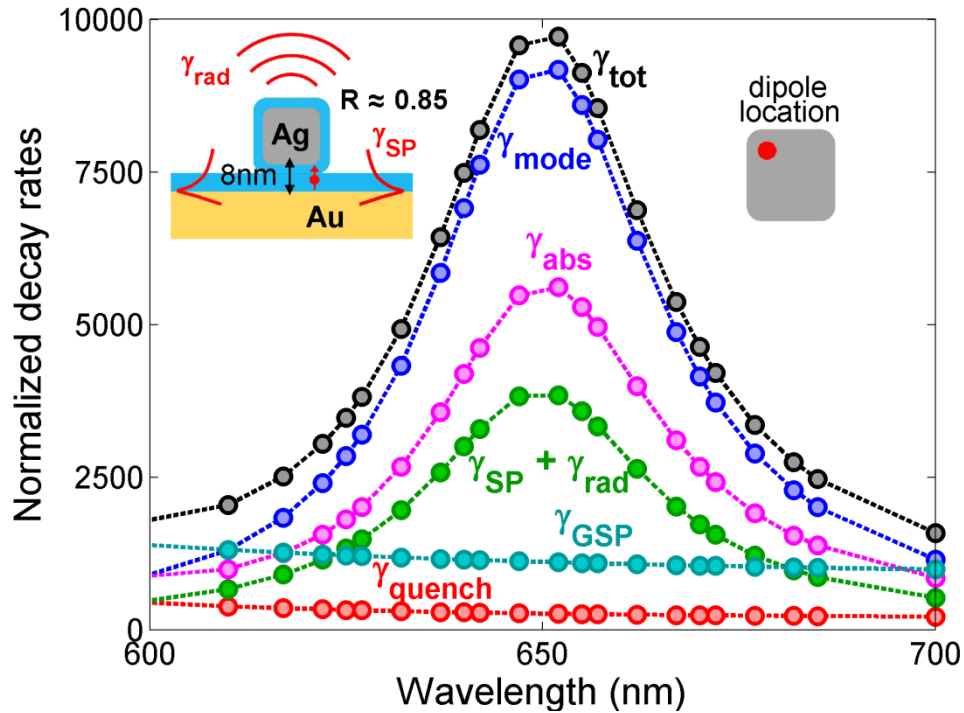


**Figure 4. Analysis of the nanocube antenna.** Calculated normalized decay rates of a vertical electric dipole at the corner (insets) of the antenna as a function of the wavelength.  $\gamma_{tot}$ ,  $\gamma_{mode}$  (decay into fundamental magnetic mode),  $\gamma_{abs}$  (antenna absorption),  $\gamma_{rad} + \gamma_{SP}$  (sum of the radiative and SPP decay rates) and  $\gamma_{quench}$  are shown by black, blue, magenta, green, and red circles, respectively.  $\gamma_{GSP}$  (cyan) represents the decay into the gap plasmon of a planar nanogap of the same materials and gap thickness. Left inset: cross-sectional view of the nanoantenna: a silver nanocube (side length 65 nm) with a 3-nm polymer coating ( $n=1.4$ ) is placed on a gold substrate covered by a 5-nm polymer (8-nm gap). The molecule is represented as a red arrow placed in the middle of the gap. Right inset: top view of the cube showing the

position of the dipole. The frequency-dependent permittivities,  $\epsilon_{Ag}$  and  $\epsilon_{Au}$ , of silver and gold are taken from tabulated data (21),  $\epsilon_{Ag} = -17 + 1.15i$  and  $\epsilon_{Au} = -9.7 + 1.04i$  @  $\lambda = 650$  nm.

We have also calculated the normalized decay  $\gamma_{mode}$  into the fundamental magnetic-dipolar nanocube mode (12, 25) using the formalism developed in (29, 30). Owing to its very small mode volume,  $V = (84,000 + 8,000i)$  nm<sup>3</sup>, and its 4-fold rotational symmetry degeneracy, 95% of the total decay is actually funneled into this resonance mode at the resonance frequency. In addition, using an open source code that allows us to calculate the radiation diagrams of the emitted photons and surface plasmons (22), we have calculated how the magnetic mode decays. We found that ~60% of the mode energy is transformed into heat in the antenna, and the remaining 40% equally decays into free-space photons and SPPs that are launched on the flat metal interface surrounding the cube ( $\gamma_{rad} \approx \gamma_{SP} \approx 0.2\gamma_{tot}$ ). The quenching rate  $\gamma_{quench}$  is then calculated by subtracting a residual decay into a quadrupolar mode (31, 32) from  $\gamma_{tot} - \gamma_{mode}$ . We find that quenching is playing a negligible role, as it represents ~2% of the total decay rate at  $\lambda_0 = 650$  nm, see the red circles.

Clearly, the nanocube antenna with a facet reflectivity of 0.85 (25) belongs to the category of nanogap antennas with large facet reflectivities, i.e. case (c) in the classification of Fig. 3.

In a second step, we have performed similar analysis by scaling all the dimensions of the gap antenna. For that, we have varied the gap thickness from 4 nm to 20 nm, and for each thickness we have adapted the cube size to maintain the magnetic-dipolar resonance at  $\lambda_0 = 650$  nm. The results that are displayed in Fig. 5a with solid lines evidence that the gap thickness, that sets the balance between Ohmic heating and outgoing decay channels (i.e.,  $\gamma_{rad}$  and  $\gamma_{SP}$ ), plays an important role for the performance. As the thickness reduces, the gap-plasmon reflectivity increases due to enhanced impedance mismatches at the facet and accordingly, the total decay rate increases. However, the reflectivity increase reduces coupling to outgoing decay channels and the enhancement of the total decay rates is associated with a drop of the extraction efficiency. For the sake of comparison, in Fig. 5b, we

display the total decay rate and the efficiency of a perfectly-tapered antenna (case (a) of the classification in Fig. 3), predicted from planar nanogap calculations by assuming that the total decay rate  $\gamma_{tot}$  of the antenna is the total decay rate of the planar nanogap with a gap thickness equal to the mouth thickness of the antenna and that the radiative decay rate  $\gamma_{rad}$  of the antenna corresponds to gap-plasmon decay rate  $\gamma_{GSP}$  of the stack (this corresponds to an upper bound for which it is assumed that the gap plasmons can be totally converted into photons). As shown by a comparison between Figs. 5a and 5b, smaller decay rates are achieved with the tapered antenna due to the absence of cavity effect, but significantly larger efficiency are also obtained. Even if the predictions for nanogap antennas are optimistic (they more represent an upper bound for the efficiency), the comparison evidences that flat nanogap antennas are particularly attractive for accelerating the spontaneous emission, but are somewhat limited with respect to extraction efficiency. Achieving large rate enhancements and large efficiencies both together will rely on our ability to increase the coupling to gap-plasmon modes while maintaining small cavity-induced absorption with engineered facet reflectivities.

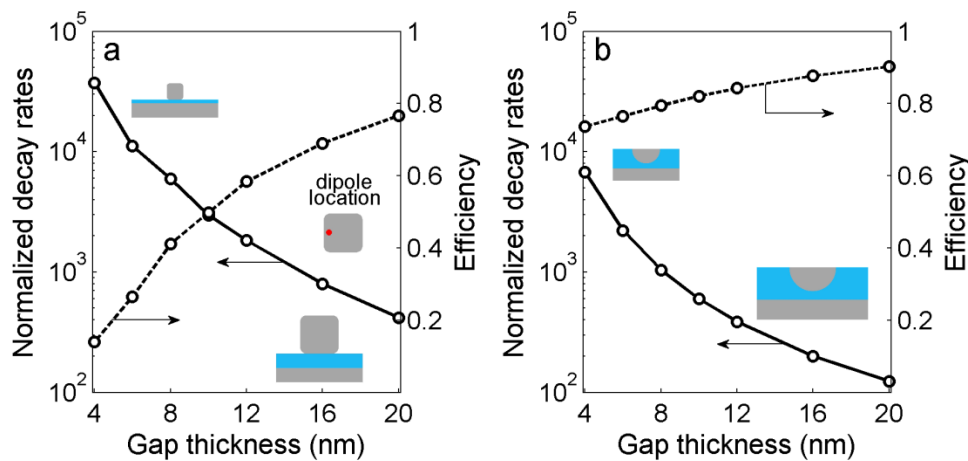


**Figure 5. Patch versus tapered-nanogap antennas with polymer gaps. (a)** Patch antennas. The calculations are performed for a vertical electric dipole located close to the center of the antenna facet (inset). The cube size varies with the gap thickness to maintain the resonance at  $\lambda_0 = 650$  nm (side lengths are 47, 56, 65, 70, 75, 80 and 85 nm, for gap thickness  $g = 4, 6, 8, 10, 12, 16$  and 20 nm). **(b)** Perfectly tapered-nanogap antennas. The performances are predicted with planar-nanogap calculations by

assuming perfect tapering of the gap-plasmon emission into radiative photons. In **(a)** and **(b)**, the normalized total decay rates and the efficiencies are shown with solid and dashed curves, respectively.

## 5. Concluding discussion

Emitting photonic devices with quantum emitters embedded in nanogaps for operation at visible and near-infrared frequencies can provide large Purcell factors and good efficiencies, because the decay into slow gap-plasmons is considerably boosted, and quenching is overcome. This is particularly true for gaps with high-refractive-index insulators sandwiched between good metals, since the branching ratio  $\propto \varepsilon_d / \text{Im}(\varepsilon_m(\omega))$  between gap-plasmon decay rates and quenching rates reach values as large as 80% for semiconductor gaps operated at near-infrared frequencies. The dominant character of plasmonic decays for small gaps has a direct impact on the design and performance of nanogap emitting devices. First, the high decay rates found in planar nanogaps can be harnessed to realize tapered antennas (Fig. 3a) offering strong Purcell factors ( $\approx 10^2$ – $10^3$ ) and large extraction efficiencies limited by the branching ratio between gap-plasmon decay rates and quenching rates, see Eq. (1). Second, even larger Purcell factors can be even achieved in nanogap cavities (Fig. 3c), which exhibit strong resonances owing to strong reflection of gap plasmons at the cavity facets. In return, the extraction efficiency is significantly reduced by the cavity absorption, as indicated by the analysis of the state-of-the-art nanocube devices. Third, a better balance between Purcell enhancement and extraction efficiency may be reached with nanogap antennas with engineered facet reflectivities (Fig. 3b) for which a delicate engineering of the facets and a precise choice of the gap and metal materials may lead to acceleration decay rates greater than  $10^3$  with significant extraction  $\approx 50\%$ .

Certainly, the main strength of nanogap light emitting devices is the capability to boost the spontaneous emission rate over a broad bandwidth with potentially easy electrical contacting. This might be useful for increasing quantum yield. However, the present analysis seems to indicate that it will be hard to achieve extremely high efficiencies ( $\approx 1$ ), as required for some quantum-information protocols, and that the branching of Eq. 3 appears as a barrier for the extraction efficiency which will be difficult to overcome.

## ASSOCIATED CONTENT

### Supporting Information.

In the supporting information, some technical details are provided.

(1) Indirect calculation of quenching. (2) Verification of the indirect quenching calculation and localized nature of the quenched fields. (3) Asymptotic expression of  $\gamma_{GSP}$  for MIM stacks with vanishing gap thickness. This material is available free of charge via the Internet at <http://pubs.acs.org>.

## AUTHOR INFORMATION

### Corresponding Author

\*E-mail: philippe.lalanne@institutoptique.fr

### Notes

The authors declare no competing financial interest.

**Acknowledgment.** The authors thank Jean-Paul Hugonin for computational helps. R. F. acknowledges financial support from the French "Direction Générale de l'Armement" (DGA).

## References.

1. Schuller, J.A.; Barnard, E.S.; Cai, W.; Jun, Y.C.; White, J.S.; Brongersma, M.I. *Nature Mater.* **2010**, *9*, 193-204.
2. Halas, N. J.; Lal, S.; Chang, W.-S.; Link, S.; Nordlander, P. *Chem. Rev.* **2011**, *111*, 3913–3961.
3. Roxworthy, B. J.; Ko, K. D.; Kumar, A.; Fung, K. H.; Chow, E. K. C.; Liu, G. L.; Fang, N. X.; Toussaint Jr., K. C. *Nano Lett.* **2012**, *12*, 796.
4. Ishi, T.; Fujikata, T.; Makita, K.; Baba, T.; Ohashi, K. *Jpn. J. Appl. Phys.* **2005**, *44*, 364-366.
5. Valentine, J.; Zhang, S.; Zentgraf, T.; Ulin-Avila, E.; Genov, D. A.; Bartal, G.; Zhang, X., *Nature* **2008**, *455*, 376-379.
6. Yang, J.; Sauvan, C.; Liu, H. T.; Lalanne, P. *Phys. Rev. Lett.* **2011**, *107*, 043903.
7. Kim, S.; Jin, J.; Kim, Y.-J.; Park, I.-Y.; Kim, Y.; Kim, S.-W. *Nature* **2008**, *453*, 757-760.
8. Agio, M. *Nanoscale* **2012**, *4*, 692.
9. Eggleston, M. S.; Messer, K.; Zhang, L.; Yablonovitch, E.; Wu, M. C. *Proc. Natl. Acad. Sci.* **2015**, *112*, 1704-1709.
10. Akselrod, G. M.; Argyropoulos, C.; Hoang, T. B.; Ciraci, C.; Fang, C.; Huang, J.; Smith, D. R.; Mikkelsen, M. H. *Nature Photon.* **2014**, *8*, 835.
11. Russell, K. J.; Liu, T.-L.; Cui, S.; Hu, E. L. *Nature Photon.* **2012**, *6*, 459.
12. Rose, A.; Hoang, T. B.; McGuire, F.; Mock, J. J.; Ciraci, C.; Smith, D. R.;

- Mikkelsen, M. H. *Nano Lett.* **2014**, *14*, 4797.
13. Koenderink, A. F. *Nano Lett.* **2009**, *9*, 4228-4233.
  14. Gan, C. H.; Hugonin, J.-P.; Lalanne, P. *Phys. Rev. X* **2012**, *2*, 021008.
  15. Khajavikhan, M.; Simic, A.; Katz, M.; Lee, J. H.; Slutsky, B.; Mizrahi, A.; Lomakin, V.; Fainman, Y. *Nature* **2012**, *482*, 204.
  16. Oulton, R. F.; Sorger, V. J.; Zentgraf, T.; Ma, R.-M.; Gladden, C.; Dai, L.; Bartal, G.; Zhang, X. *Nature* **2009**, *461*, 629.
  17. Lu, Y.-J.; Wang, C.-Y.; Kim, J.; Chen, H.-Y.; Lu, M.-Y.; Chen, Y.-C.; Chang, W.-H.; Chen, L.-J.; Stockman, M. I.; Shih, C.-K.; Gwo, S. *Nano Lett.* **2014**, *14*, 4381.
  18. Jun, Y. C.; Kekatpure, R. D.; White, J. S.; Brongersma, M. L. *Phys. Rev. B* **2008**, *78*, 153111.
  19. Ford, G. W.; Weber, W. H. *Phys. Rep.* **1984**, *113*, 195.
  20. Collin, R. E. *IEEE Antennas Propag. Mag.* **2004**, *46*, 64.
  21. Palik, E. D. *Handbook of Optical Constants*; Academic Press: San Diego, 1998.
  22. Yang, J.; Hugonin, J.-P.; Lalanne, P. , Near-to-far field transformations for radiative and guided waves, arXiv e-Print archive 2015.
  23. Miyazaki, H. T.; Kurokawa, Y. *Phys. Rev. Lett.* **2006**, *96*, 097401.
  24. Bozhevolnyi, S. I.; Søndergaard, T. *Opt. Express* **2007**, *15*, 10869.
  25. Yang, J.; Sauvan, C.; Jouanin, A.; Collin, S.; Pelouard, J.-L.; Lalanne, P. *Opt. Express* **2012**, *20*, 16880.
  26. Fernández-Domínguez, A. I.; Maier, S. A.; Pendry, J. B. *Phys. Rev. Lett.* **2010**, *105*, 266807.
  27. Yamamoto, N.; Ohtani, S.; García de Abajo, F. J. *Nano Lett.* **2011**, *11*, 91.
  28. Mubeen, S.; Zhang, S.; Kim, N.; Lee, S.; Krämer, S.; Xu, H.; Moskovits, M. *Nano Lett.* **2012**, *12*, 2088.
  29. Sauvan, C.; Hugonin, J.-P.; Maksymov, I. S.; Lalanne, P. *Phys. Rev. Lett.* **2013**, *110*, 237401.
  30. Bai, Q.; Perrin, M.; Sauvan, C.; Hugonin, J.-P.; Lalanne, P. *Opt. Express* **2013**, *21*, 27371.
  31. Akselrod, G. M.; Ming, T.; Argyropoulos, C.; Hoang, T. B.; Lin, Y.; Ling, X.; Smith, D. R.; Kong, J.; Mikkelsen, M. H. *Nano Lett.* **2015**, *15*, 3578.
  32. Britt Lassiter, J.; McGuire, F.; Mock, J. J.; Ciraci, C.; Hill, R. T.; Wiley, B. J.; Chilkoti, A.; Smith, D. R. *Nano Lett.*, **2013**, *13*, 5866.